



ELSEVIER

Coastal Engineering 29 (1996) 101–121

**COASTAL  
ENGINEERING**

# The growth of fetch limited waves in water of finite depth. Part 3. Directional spectra

I.R. Young <sup>a,1</sup>, L.A. Verhagen <sup>b,2</sup>, S.K. Khatri <sup>a,3</sup>

<sup>a</sup> School of Civil Engineering, University College, Univ. of NSW, Canberra, A.C.T. 2600, Australia

<sup>b</sup> HASKONING, P.O. Box 151, 6500 AD Nijmegen, Netherlands

Received 10 November 1995; accepted 4 May 1996

---

## Abstract

The analysis of a comprehensive data set of fetch limited finite depth directional wave spectra is presented. The data show that the spectra are narrowest at the frequency of the spectral peak and gradually broaden for frequencies both greater than and less than that of the peak. The directional spreading is found to be a function of  $f/f_p$ , where  $f$  is frequency and  $f_p$  the frequency of the spectral peak. In addition, the present data reveal consistently broader spreading than comparable deep water data. Hence, it is concluded that finite depth effects lead to an increase in the directional spreading of the spectrum. An analysis of the nonlinear coupling of wavenumber components within the spectrum indicates that such effects may lead to enhanced directional spreading of spectra as the water depth decreases, consistent with the present data set.

*Keywords:* Waves; Finite depth; Spectrum; Directional spreading

---

## 1. Introduction

A comprehensive understanding of the directional properties of wind generated ocean waves is important for engineering applications such as the design of offshore structures and coastal sediment transport. In particular, transformation processes such as diffraction, refraction and reflection are greatly influenced by the directional characteristics of

---

<sup>1</sup> Email: iry@wavcs.ce.adfa.oz.au

<sup>2</sup> Email: vla@fugro-inpark.nl

<sup>3</sup> Email: skk@waves.ce.adfa.oz.au

the waves. These requirements necessitate an understanding of the directional spectrum in both deep and finite depth water. Although there is a relatively comprehensive data base of fetch limited spectra in deep water, a similar situation does not exist in finite depth situations. Indeed, no comprehensive data set of fetch limited, finite depth directional spectra has, to date, been published.

This paper presents an extensive data set of directional spectra obtained under fetch limited conditions in water of finite depth. The data were collected as part of the Lake George finite depth study described by Young and Verhagen (1996a,b). The data were obtained with a seven element directional array which provides significantly higher directional resolving power than traditional pitch-roll buoys.

The arrangement of this paper is as follows. In Section 2 a brief review of previous measurements of directional spectra is presented followed by a description of the present experimental design in Section 3. A full description of the available data and its characteristics is presented in Section 4. Previously proposed parametric forms for the representation of directional spectra are explored in the context of the present data in Section 5. The potential role of nonlinear interactions in explaining differences between these finite depth results and previous deep water data is discussed in Section 6. Finally the conclusions of the study appear in Section 7.

## **2. Directional distribution of wind waves**

Two general methods have been utilized for the measurement of directional wave spectra; remote sensing and insitu instruments. Remote sensing techniques include both passive photographic techniques in the visual frequency range and a variety of radar systems. Directional or two-dimensional wavenumber spectra were first obtained using aerial photography by Cote et al. (1960). These data were followed by the first three-dimensional spectra (i.e. wavenumber–frequency) obtained by Garrett (1970). Numerous other accounts of the measurement of both two and three-dimensional spectra followed these pioneering studies (Tyler et al., 1974; Wu, 1977; Schuler, 1978; Fontanel and De Staerke, 1980; McLeish et al., 1980; Pawka et al., 1980; Trizna et al., 1980; Holthuijsen, 1983; Irani et al., 1981; Young et al., 1985; Banner, 1990). None of these studies provides a comprehensive understanding of the directional spreading of wind waves. Many of the studies consider only a small number of spectra and span a relatively small parameter range. In addition, two-dimensional wavenumber spectra include a  $180^\circ$  directional ambiguity. Although this can be resolved with little difficulty at low wavenumber, where the spreading is narrow, at high wavenumber the spreading can exceed  $180^\circ$  and the ambiguity cannot be removed without prior assumptions. In addition, many of the airborne techniques have insufficient resolution to resolve high wavenumber components.

In situ techniques utilize multiple measurements of wave properties such as elevation, velocity, acceleration, slope or pressure. Irrespective of the number of quantities measured, the problem is invariably underdefined and certain assumptions are necessary to determine the directional spectrum consistent with the measured quantities (Young,

1994). Despite this shortcoming, insitu instruments can be operated for extended periods of time and hence collect extensive data sets. Numerous reports of the measurement of directional spectra using such instruments exist (e.g. Forristall et al., 1978; Buchan et al., 1984; Kobune et al., 1985; Ewing and Laing, 1987).

Three extensive data sets of fetch limited deep water directional spectra have been obtained with insitu instruments (Mitsuyasu et al., 1975; Hasselmann et al., 1980; Donelan et al., 1985).

It is common practice to consider the directional spectrum,  $F(f, \theta)$ , where  $f$  is frequency and  $\theta$  the direction of wave propagation, in terms of the one-dimensional spectrum,  $F(f)$ , as (Longuet-Higgins et al., 1963)

$$F(f, \theta) = F(f) D(f, \theta) \quad (1)$$

The directional spreading function,  $D(f, \theta)$  must satisfy the condition

$$\int_{-\pi}^{\pi} D(f, \theta) d\theta = 1 \quad (2)$$

Mitsuyasu et al. (1975) considered data collected with a cloverleaf buoy which measured six quantities related to the surface wave field (the vertical acceleration of the water surface,  $\eta_{tt}$ , the wave slope,  $\eta_x$ ,  $\eta_y$  and the surface curvature,  $\eta_{xx}$ ,  $\eta_{yy}$ ,  $\eta_{xy}$ ). Their analysis procedure, considered only the surface acceleration and slope information, reducing the data to that which would be collected with a pitch-roll buoy. Following Longuet-Higgins et al. (1963) they represented  $D(f, \theta)$  in the form

$$D(f, \theta) = Q(s) \cos^{2s} \frac{[\theta - \bar{\theta}(f)]}{2} \quad (3)$$

where  $Q(s)$  is a normalization factor required to satisfy Eq. (2) and  $\bar{\theta}$  is the mean wave direction at frequency  $f$ . Based on their data, Mitsuyasu et al. (1975) parameterized  $s$  as

$$s = \begin{cases} s_p \left( \frac{f}{f_p} \right)^5 & f < f_p \\ s_p \left( \frac{f}{f_p} \right)^{-2.5} & f \geq f_p \end{cases} \quad (4)$$

where  $s_p$  is the value of  $s$  at the frequency of the spectral peak,  $f_p$ , given by

$$s_p = 11.5 \left( \frac{U_{10}}{C_p} \right)^{-2.5} \quad (5)$$

$C_p = g/\omega_p$  is the deep water phase speed of components at the spectral peak,  $\omega_p = 2\pi f_p$  and  $U_{10}$  is the wind speed at a reference height of 10 m.

Hasselmann et al. (1980) considered pitch/roll buoy data, also representing their data in the form of Eq. (3) but with a different parameterization for  $s$

$$s = \begin{cases} 6.97 \left( \frac{f}{f_p} \right)^{4.06} & f < 1.05 f_p \\ 9.77 \left( \frac{f}{f_p} \right)^{\mu} & f \geq 1.05 f_p \end{cases} \quad (6)$$

where  $\mu$  has a weak dependence on wave age

$$\mu = -2.33 - 1.45 \left( \frac{U_{10}}{C_p} - 1.17 \right) \quad (7)$$

The general form for the spreading function described by Eq. (3) has also been supported by stereophotographic observations by Holthuijsen (1983).

Based on data from an array of 14 wave gauges, Donelan et al. (1985) found that the form described by Eq. (3) did not adequately represent their data and adopted the alternative form

$$D(f, \theta) = 0.5 \beta \operatorname{sech}^2 \beta [\theta - \bar{\theta}(f)] \quad (8)$$

They found that  $\beta$  varied as a function of non-dimensional frequency,  $f/f_p$ . Their data, however, extended only to  $f/f_p = 1.6$  and beyond this point they assumed  $\beta$  was constant. Banner (1990) reviewed this conclusion in the context of high frequency stereophotographic data and concluded that the assumption that  $\beta = \text{constant}$  for  $f/f_p > 1.6$  was unreasonable. He proposed a formulation for  $\beta$  beyond  $1.6 f_p$  which is combined with the Donelan et al. (1985) parameterizations for  $f < 1.6 f_p$  in Eq. (9) below

$$\beta = \begin{cases} 2.61 \left( \frac{f}{f_p} \right)^{1.3} & 0.56 < f/f_p < 0.95 \\ 2.28 \left( \frac{f}{f_p} \right)^{-1.3} & 0.95 < f/f_p < 1.6 \\ 10 \{-0.4 + 0.8393 \exp[-0.567 \ln((f/f_p)^2)]\} & f/f_p > 1.6 \end{cases} \quad (9)$$

The directional spreading proposed by these three representations vary significantly, particularly near the spectral peak. The result of Donelan et al. (1985), Eq. (9), is significantly narrower than the other forms. Donelan et al. (1985) attributed this to the poor directional resolving power of the buoy data utilized by both Mitsuyasu et al. (1975) and Hasselmann et al. (1980) and the Fourier expansion method adopted in both these analyses. Young (1994) has made a detailed comparison of all three proposed directional forms as well as the instrumentation and analysis techniques used. The final

conclusion was that the pitch-roll buoy data must yield directional forms which are broader than the results from the multiple gauge array of Donelan et al. (1985).

Both Mitsuyasu et al. (1975) and Hasselmann et al. (1980) proposed a dependence on the inverse wave age  $U_{10}/C_p$  as well as  $f/f_p$ . Their data, however, span only a relatively small range of  $U_{10}/C_p$ . In contrast, Donelan et al. (1985) could find no systematic dependence on  $U_{10}/C_p$  from a data set which spanned a much wider parameter range.

### 3. Instrument design

The data described in this paper form part of a larger finite depth, fetch limited evolution experiment described in Young and Verhagen (1996a) (henceforth Part I) and Young and Verhagen (1996b) (henceforth Part II). The data were obtained with a spatial array consisting of seven gauges as shown in Fig. 1. The gauges were arranged in the form of a “Mercedes Star” with a central gauge and two rings of three gauges at radii of 0.20 m and 0.55 m respectively. The gauges were coincidentally sampled at 8 Hz and the directional spectrum formed using the Maximum Likelihood Method (MLM) (Isobe et al., 1984; Young, 1994). Time series of duration 30 min. were collected from each gauge. These time series were sub-divided into 112 blocks, each of 128 points for subsequent Fourier transformation as part of the MLM analysis.

The first step in determining the directional wave spectrum using the MLM from the

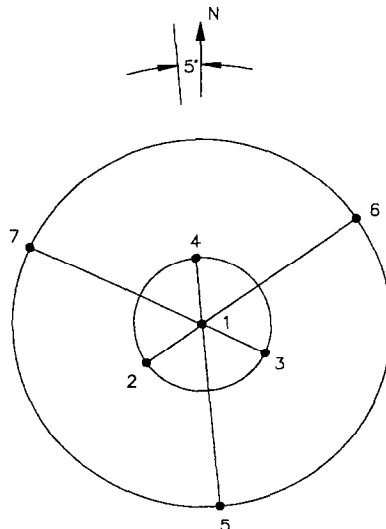


Fig. 1. Geometry of the 7 element directional array. Elements 2, 3 and 4 were at a radius of 0.20 m and elements 5, 6 and 7 were at a radius of 0.55 m.

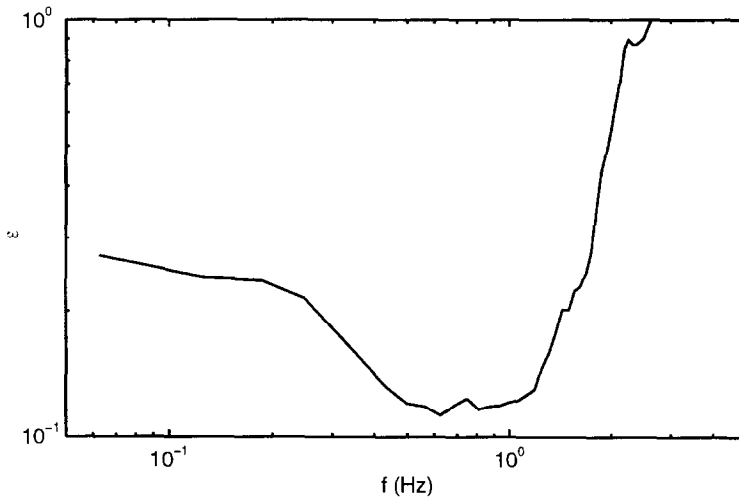


Fig. 2. The mean relative error  $\epsilon$  (Eq. (10)) for the directional array as a function of frequency. The frequency range of interest is  $0.1 \text{ Hz} < f < 1 \text{ Hz}$  for which  $\epsilon$  is small and hence the array geometry is optimal.

coincidentally sampled water surface elevation records for each of the gauges is to form the cross-spectra between all array elements. For an assumed directional spectral form, the cross spectra can be determined numerically. These cross-spectra can then be processed by the MLM and the resulting directional spectrum compared with the initial input form. In order to assess the directional resolving power of the present array and analysis technique, a spreading function of the form described by Eq. (3) was assumed with a constant value of  $s = 10$  at all frequencies. A small amount (1% of maximum spectral ordinate) of incoherent noise was also added to each spectral ordinate.

The performance of the instrument and analysis technique can be assessed in terms of the mean relative error,  $\epsilon(f)$

$$\epsilon(f) = \frac{\int |F(f, \theta) - \hat{F}(f, \theta)| d\theta}{\int F(f, \theta) d\theta} \quad (10)$$

where  $F(f, \theta)$  is the initial analytical test spectral form and  $\hat{F}(f, \theta)$  is the form recovered by the MLM analysis.

The values of  $\epsilon(f)$  are shown as a function of frequency in Fig. 2. Peak spectral frequencies for the present data set are typically 0.3 Hz. It is desired to obtain reliable directional spectra within the range  $0.3 < f/f_p < 3$  or  $0.1 \text{ Hz} < f < 1 \text{ Hz}$ . As can be seen in Fig. 2, the array geometry is optimally designed to resolve this frequency range. At low frequencies the array performance is limited by the measurement accuracy of the array elements, whereas at high frequencies ( $> 2 \text{ Hz}$ ) the finite spacing between array elements leads to spatial aliasing. As demonstrated by Young (1994), all array geometries and analysis techniques yield directional spectra  $[\hat{F}(f, \theta)]$  broader than the input form  $[F(f, \theta)]$ .

#### 4. Available data

Data collection was controlled by a computer located adjacent to the directional array. As each 30 min. logging session generated approximately 600 kbytes of data, storage was an important consideration. To maximize available storage, logging sessions were initiated remotely through a radio modem link. When conditions appeared suitable, the radio modem link could be used to remotely switch on the computer and initiate a logging session. Data were down loaded on regular maintenance visits to the array (see Part I).

During the measurement period (approximately 18 months), the water depth varied between 1.8 m and 2.4 m and data were collected for wind speeds ranging between 3 m/s and 15 m/s. A total of 156 directional spectra were recorded with the array during this experimental period. As described in Part I, Lake George is approximately 20 km long in the north/south direction by 10 km wide in the east/west direction. The most common wind direction was from the west with easterlies being the next most frequent. Northerlies and southerlies are quite rare. When wind directions deviated by angles of more than  $\pm 10^\circ$  from the line normal to the long east/west shorelines, the resulting directional spectra tended to be directionally skewed. The waves tend to propagate more in the direction of the long north/south fetch in such situations, rather than in the wind direction. This trend was confirmed by visual observations. Similar results were also reported by Holthuijsen (1983) and Donelan et al. (1985). Such spectra were excluded from further analysis by considering only those cases for which the wind direction was within  $\pm 10^\circ$  of shore normal. The resulting data set consisted of 58 directional spectra.

Parameters defining the data set are summarized in the distribution histograms shown in Figs. 3 and 4. Fig. 3 shows the distribution of the inverse wave age,  $U_{10}/C_p$  for the

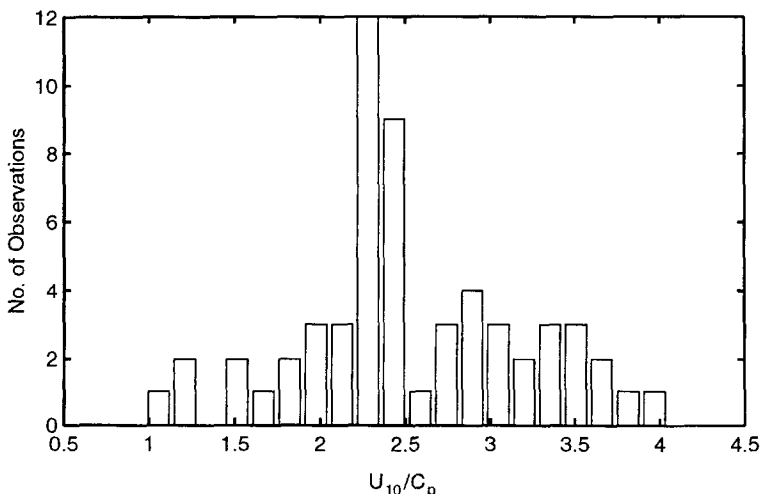


Fig. 3. Distribution of the directional data based on recorded values of the inverse wave age,  $U_{10}/C_p$ .

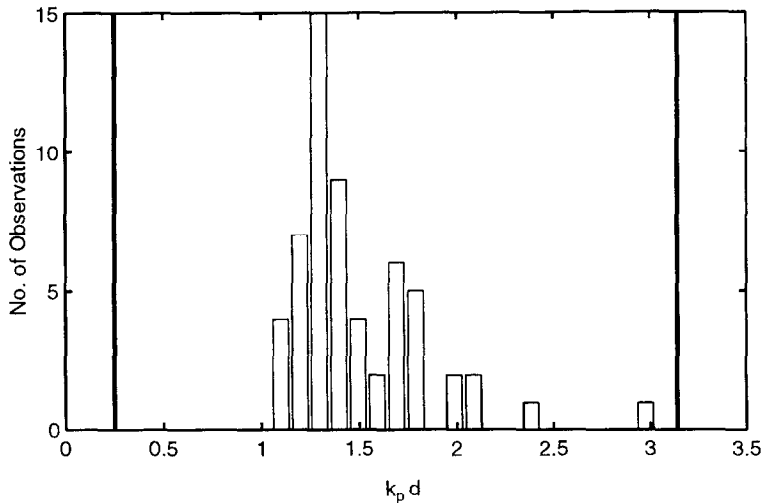


Fig. 4. Distribution of the directional data based on recorded values of the parameter  $k_p d$ . The two thick vertical lines mark the deep (right) and shallow (left) water limits for linear wave theory.

data set. The large majority of the data are clustered near  $U_{10}/C_p \approx 2.3$ , although the data set covers cases from fully developed spectra with  $U_{10}/C_p \approx 1$  to very young and highly forced cases with  $U_{10}/C_p \approx 4$ . This is a significantly broader parameter range than that utilized by either Mitsuyasu et al. (1975) or Hasselmann et al. (1980) and is similar to the parameter range for the Donelan et al. (1985) data.

The effects of finite depth can be quantified in terms of the non-dimensional parameter  $k_p d$ , where  $k_p$  is the wavenumber of the spectral peak and  $d$  is the water depth. Fig. 4 shows the distribution of  $k_p d$  values for the data set. The vast majority of the data is in the range  $1 < k_p d < 2$ . Values of  $k_p d > \pi$  are generally considered to represent deep water conditions whilst  $k_p d < 0.25$  represent shallow water. Hence, the entire data set is in transitional water depth. Consequently, the spectra would be expected to be influenced by finite depth effects (see Part II). The relatively narrow distribution of  $k_p d$ , however, precludes the possibility of directly investigating the evolution of the directional spreading from deep to finite depth water.

## 5. Parametric representation of the data

### 5.1. Determination of appropriate model

It is desired to investigate the applicability of the two proposed spreading models  $\cos^2\theta/2$  and  $\text{sech}^2\beta\theta$ . A number of different techniques have been reported for the fitting of such analytical forms to the data. Mitsuyasu et al. (1975) and Hasselmann et al. (1980) analyzed their buoy data using the Fourier Expansion Method (Longuet-Higgins et al., 1963; Young, 1994) and determined the value of  $s$  from the first 2 components of

the Fourier expansion. Donelan et al. (1985) compared this approach with one in which the directional form was matched to the half-power points of the measured spreading function. It was argued that matching the half-power points was more meaningful since interest is concentrated on the energetic region of the directional distribution. This technique appeared to reduce the scatter in the data.

In addition to these techniques, application of a nonlinear least squares fit [Levenberg–Marquardt method, Press et al. (1986)] was also investigated with the present data. The least squares approach, which fits the analytical form to the full directional distribution obtained from the MLM analysis, consistently yielded results with least scatter and has been adopted for subsequent analysis.

The MLM derived spectra were initially normalized to ensure a maximum ordinate of one at each frequency

$$\hat{D}(f, \theta) = \frac{\hat{F}(f, \theta)}{\hat{F}_{\max}(f, \theta_{\max})} \quad (11)$$

where  $\hat{F}(f, \theta)$  is the directional spectrum derived from the MLM analysis and  $\hat{F}_{\max}(f, \theta_{\max})$  is the maximum ordinate of the directional spectrum, which occurs in direction  $\theta_{\max}$ . To the normalized spectra, described by Eq. (11), functions of the following form were fitted independently for each frequency.

$$A(f, \theta) = \begin{cases} \cos^{2s(f)} \left[ \frac{\theta - \bar{\theta}(f)}{2} \right] \\ \operatorname{sech}^2 \beta(f) [\theta - \bar{\theta}(f)] \end{cases} \quad (12)$$

In each case, the least squares technique determined two parameters at each frequency ( $s$  and  $\bar{\theta}$  or  $\beta$  and  $\bar{\theta}$ ). The ‘‘goodness of fit’’ of each of the functions to the data was determined through the calculation of the error,  $\varepsilon$

$$\varepsilon(f) = \frac{1}{N} \sqrt{\sum_{i=1}^N \Delta^2(f, \theta_i)} \quad (13)$$

where

$$\Delta(f, \theta_i) = \hat{D}(f, \theta_i) - A(f, \theta_i) \quad (14)$$

and  $N$  is the total number of directional bands in the discrete spectral representation.

If the value of  $\varepsilon$  exceeded 0.01, it was considered that the fit to the data was poor and the resulting values of  $s$  or  $\beta$  were discarded. This occasionally occurred at high frequencies since the relative noise level in the data increased with frequency. The resulting values of  $s$  and  $\beta$  are shown as a function of the normalized frequency,  $f/f_p$  in Fig. 5. Both formulations of the spreading function yield qualitatively similar results, indicating the spectrum is narrowest at the spectral peak frequency and broadens at frequencies both larger and smaller than the peak value. Values of  $s$  range over a factor of 10 whilst  $\beta$  varies by only a little more than a factor of 2. As a result, the relative data scatter is larger for the  $\operatorname{sech}^2 \beta \theta$  function than the  $\cos^2 \theta / 2$  form. The  $\cos^2 \theta / 2$

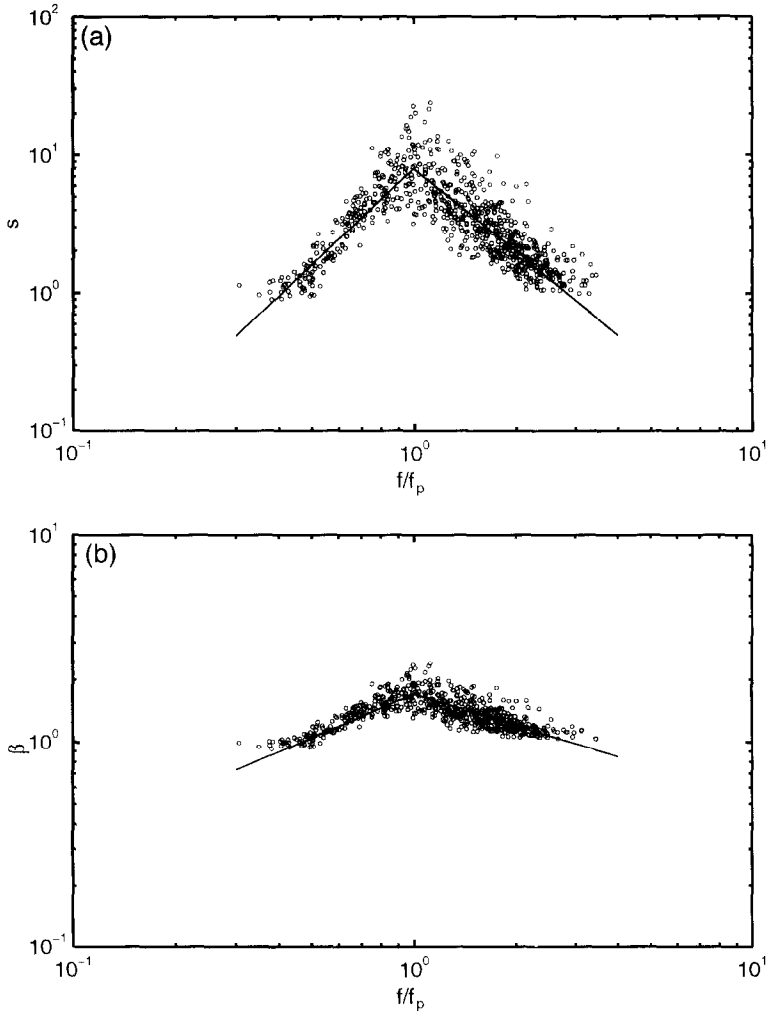


Fig. 5. (a) Values of the directional exponent  $s$  (Eq. (3)) as a function of the normalized frequency,  $f/f_p$  for the full data set. The solid lines represent a least squares fit to the data with a break point at  $f/f_p = 1$ . (b) Values of the directional parameter  $\beta$  (Eq. (8)) as a function of the normalized frequency,  $f/f_p$  for the full data set. The solid lines represent a least squares fit to the data with a break point at  $f/f_p = 1$ .

form yields correlation coefficients of 0.89 and  $-0.67$  for the two sections  $f/f_p < 1$  and  $f/f_p > 1$ , respectively. In contrast, the  $\text{sech}^2\beta\theta$  form yields slightly smaller values of 0.78 and  $-0.62$ , respectively. This is the opposite result, to that obtained for deep water conditions by Donelan et al. (1985). As will be shown later, the Donelan et al. (1985) results are narrower than those shown in Fig. 5. In addition, the Donelan et al. (1985) data were limited to  $f/f_p < 1.6$ . Unlike, the  $\cos^2\theta/2$  function,  $\text{sech}^2\beta\theta$  is not a circular function. Therefore, a discontinuity exists in the  $\text{sech}^2\beta\theta$  directional spreading at

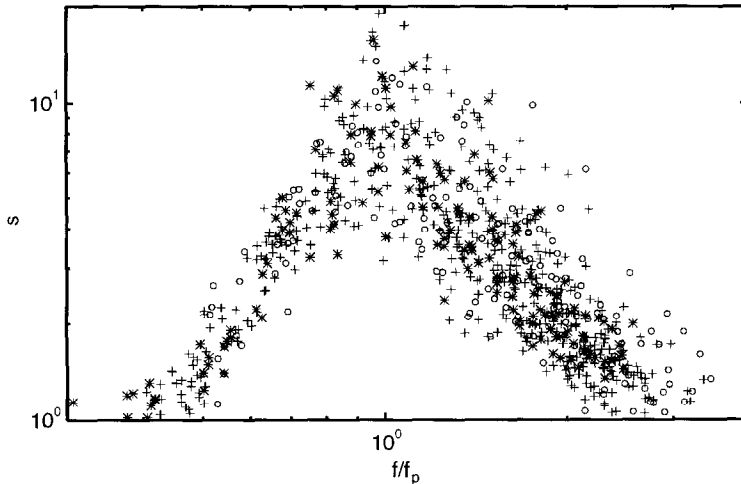


Fig. 6. Values of the directional exponent  $s$  (Eq. (3)) as a function of the normalized frequency,  $f/f_p$ . Values have been partitioned based on inverse wave age,  $U_{10}/C_p$ ,  $1 < U_{10}/C_p \leq 2$  — \*;  $2 < U_{10}/C_p \leq 3$  — +;  $U_{10}/C_p > 3$  — ○.

$|\theta - \bar{\theta}| = \pi$ . For broad directional spreading, the energy in the vicinity of the discontinuity can be significant. This is one reason for the relatively poorer performance of the  $\text{sech}^2\beta\theta$  spreading when applied to the present data set. For this reason, subsequent attention will concentrate on the  $\cos^2\theta/2$  form.

### 5.2. Wave age dependence

Mitsuyasu et al. (1975) and Hasselmann et al. (1980) both reported the deep water directional spreading to be a function of the inverse wave age  $U_{10}/C_p$ . In contrast, the data of Donelan et al. (1985), which spanned a more extensive range of  $U_{10}/C_p$  showed no dependence on this parameter. In order to investigate whether the directional spreading of the present finite depth data set is dependent on wave age, the data set was partitioned, based on  $U_{10}/C_p$ . Fig. 6 shows  $s$  as a function of  $f/f_p$ , as in Fig. 5a, but with the data partitioned into three groups:  $1 < U_{10}/C_p \leq 2$ ,  $2 < U_{10}/C_p \leq 3$ ,  $3 < U_{10}/C_p \leq 4$ . Within the scatter of the data, no dependence on  $U_{10}/C_p$  can be seen. This result is consistent with the deep water findings of Donelan et al. (1985). Although Hasselmann et al. (1980) report a dependence on  $U_{10}/C_p$  for their deep water data, the dependence is relatively weak. They conclude that this indicates that nonlinear energy transfer dominates over both atmospheric input and dissipation in determining the directional spreading. Donelan et al. (1985) caution that these other terms may still play an important role. The lack of dependence on wave age is not a conclusive indicator that the nonlinear term dominates in determining the spreading. Banner and Young (1994), investigated the form of the directional spectrum using a numerical model with a full solution to the nonlinear source term. A wide range of forms for both the atmospheric input and dissipation were investigated. Even under this wide range of permutations to

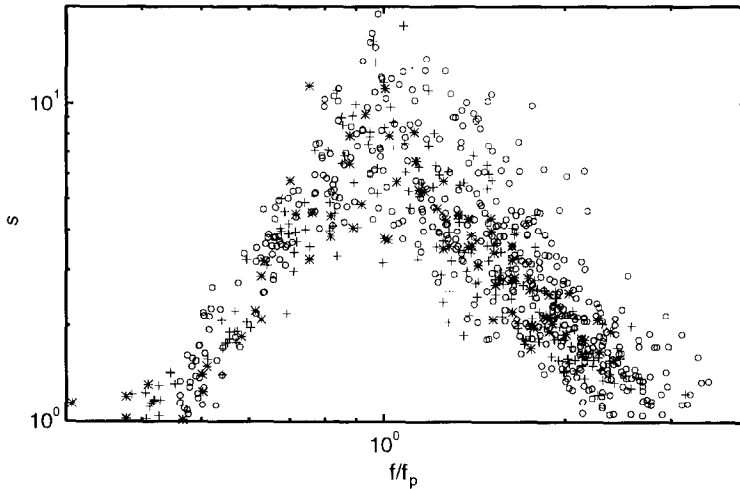


Fig. 7. Values of the directional exponent  $s$  (Eq. (3)) as a function of the normalized frequency,  $f/f_p$ . Values have been partitioned based on the relative depth parameter,  $k_p d$ .  $1.0 < k_p d \leq 1.5$  —  $\circ$ ;  $1.5 < k_p d \leq 2.0$  —  $+$ ;  $k_p d > 2.0$  —  $*$ .

the forcing, the directional spreading remained largely constant. Hence the evidence tends to support the premise that nonlinear interactions dominate in determining the deep water spreading. The present data set extends this result to finite depth conditions.

### 5.3. Water depth dependence

The principal reason for collecting the present data set was to determine whether the directional distribution of finite depth waves differs from their deep water counterparts. In order to investigate the influence of finite depth, the results shown in Fig. 5a are re-plotted in Fig. 7 but with the data partitioned based on  $k_p d$ . The values of  $k_p d$  are divided into three groups:  $1.0 < k_p d \leq 1.5$ ,  $1.5 < k_p d \leq 2.0$ ,  $2.0 < k_p d \leq 2.5$ . There is no clear variation in the spreading as a function of  $k_p d$ . This result, however, should not be interpreted as clear evidence that depth dependence plays no role in determining the directional spreading. The present data set spans a relatively small range of  $k_p d$ , all values being in transitional water depths (see Fig. 4). Hence, it is possible that any dependence is masked by the natural scatter of the data. As will be shown later, the present data set indicates spreading significantly broader than the deep water data of Donelan et al. (1985).

### 5.4. Comparison with deep water results

As indicated in Section 3, the multi-element array utilized here, like all insitu instruments, produces spectra broader than actually occur. The extent of the artificial broadening varies with the number of sensing elements in the instrument and the

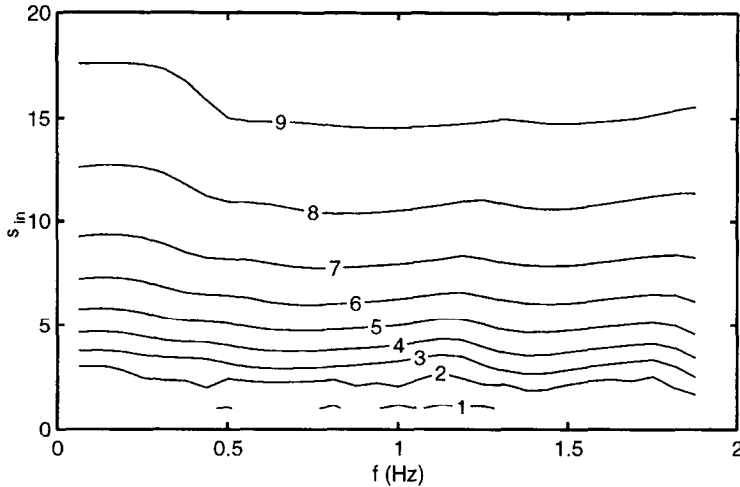


Fig. 8. Contours of the exponent  $s_{out}$  derived by the MLM analysis method for the array, as a function of the input exponent,  $s_{in}$  and frequency. As  $s_{out}$  is always less than  $s_{in}$ , the array artificially broadens the data.

analysis technique (Young, 1994). As the directional resolving properties of the present array and MLM analysis technique are known, it is possible to correct the directional spectra for this artificial broadening. A series of directional spectra with  $\cos^2\theta/2$  directional spreading were generated with values of  $1 < s < 20$ . These were used as input to the MLM analysis software, as discussed in Section 3. Values of  $s$  for the output spectra from the MLM analysis were then determined using the least squares technique described in Section 5.1. Fig. 8 shows the derived value of  $s$  ( $s_{out}$ ) as a function of the input value of  $s$  ( $s_{in}$ ) and frequency. The dependence on  $f$  is weak but the artificial broadening is strongly dependent on the width of the input spreading. Broad spectra (eg  $s \approx 1$ ) are accurately measured by the system. In contrast, narrow input spectra are significantly broadened by the analysis (e.g.  $s_{in} = 16$  would be represented by the instrumentation as  $s_{out} \approx 9$ ). As the results are largely independent of  $f$ , they were averaged over all frequencies shown in Fig. 8 to yield the relationship shown in Fig. 9. This relationship was used to correct all measured values of  $s$ .

Correcting the linear fit to the data shown in Fig. 5a yields the following form for the present finite depth data

$$s = \begin{cases} 11 \left( \frac{f}{f_p} \right)^{2.7} & f < f_p \\ 11 \left( \frac{f}{f_p} \right)^{-2.4} & f \geq f_p \end{cases} \quad (15)$$

Eq. (15) has been constrained to yield narrowest spreading at  $f/f_p = 1$ . The scatter in the data is such that the actual point of narrowest spreading cannot be determined with great accuracy. It is clearly, however, in the vicinity of the spectral peak frequency.

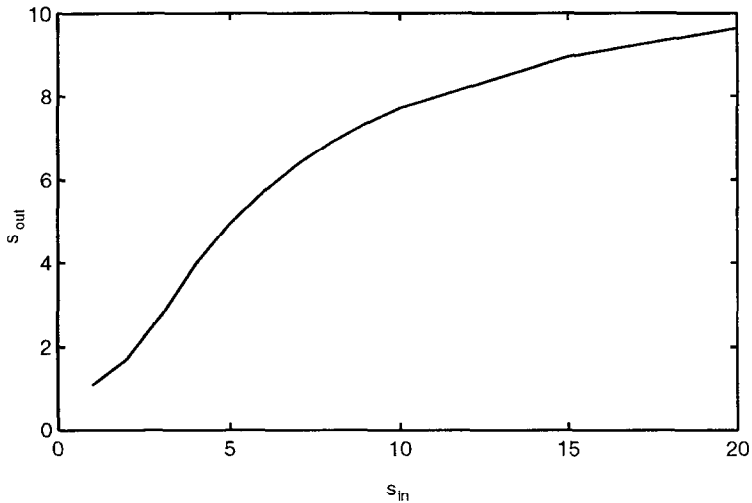


Fig. 9. Average values of  $s_{out}$  as a function of  $s_{in}$  obtained by integration of the results shown in Fig. 8 with respect to frequency. This curve was used to correct the data for artificial broadening.

Eq. (15) is shown in Fig. 10 together with the deep water results of Mitsuyasu et al. (1975), Hasselmann et al. (1980) and Donelan et al. (1985). As the results of Mitsuyasu et al. (1975) and Hasselmann et al. (1980) are both wave age dependent, mean values typical of their respective data sets have been used to construct Fig. 10 (Mitsuyasu et al.,

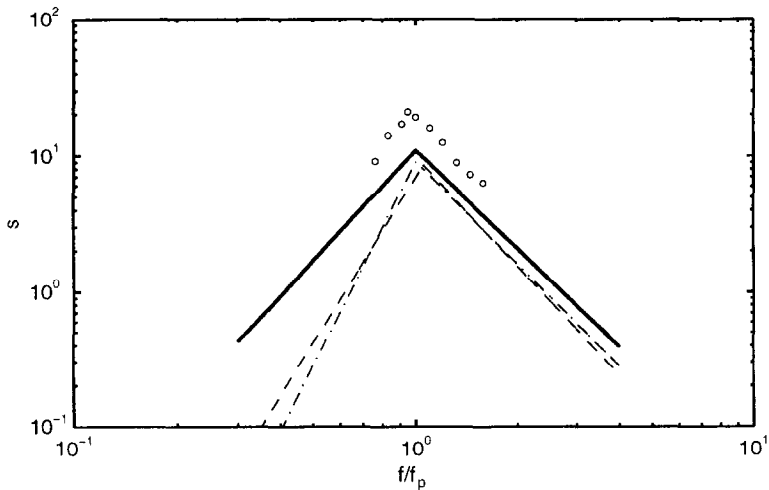


Fig. 10. The dependence of the directional exponent  $s$  for the present finite depth data as a function of  $f/f_p$  (Eq. (15)) (thick solid line). Also shown for comparative purposes are previous deep water data sets: Mitsuyasu et al. (1975) (Eq. (15)) — dash dot line; Hasselmann et al. (1980) (Eq. (15)) — dashed line; Donelan et al. (1985) — open circles.

1975 –  $U_{10}/C_p = 1.1$ ; Hasselmann et al., 1980 –  $U_{10}/C_p = 1.4$ ). As Donelan et al. (1985) provide no functional form expressed in terms of  $s$ , the result in Fig. 10 was obtained from digitizing the result given in their Fig. 30.

The present results are marginally narrower (higher  $s$ ) than those of both Mitsuyasu et al. (1975) and Hasselmann et al. (1980), they are however significantly broader than the high resolution results of Donelan et al. (1985). As explained earlier, the evidence suggests (Donelan et al., 1985; Young, 1994) that the results of both Mitsuyasu et al. (1975) and Hasselmann et al. (1980) are excessively broad due to the instrumentation and analysis technique utilized. The present result (Eq. (15)) has been corrected for artificial broadening and should have comparable resolving power to the result of Donelan et al. (1985). The inference is that finite depth wind wave spectra are broader than their deep water counterparts. Due to the relatively narrow range of  $k_p d$  spanned by the present data set a more emphatic statement cannot be made. At present it is necessary to rely on these two independent data sets (Donelan et al., 1985 — deep water; Lake George — finite depth). There is always some possibility that, in addition to water depth, there are other unknown influences responsible for the different spreading.

## 6. The role of nonlinear interactions

The evolution of the directional wave spectrum is commonly written in terms of the Radiative Transfer Equation (Gelci et al., 1957; Hasselmann, 1960; Willebrand, 1975)

$$\frac{DF(f, \theta)}{Dt} = S_{in} + S_{nl} + S_{ds} + S_b \quad (16)$$

where the source terms on the right of the equation represent; atmospheric input from the wind,  $S_{in}$ ; nonlinear interactions within the spectrum,  $S_{nl}$ ; dissipation due to white-capping,  $S_{ds}$  and interactions with the bottom,  $S_b$ . Knowledge of these source terms in deep water is less than complete and in finite depth situations, very limited. It is reasonable to assume that since the phase speed of waves in finite depth water is less than in deep water, the ratio  $U_{10}/C$  will be larger and hence the atmospheric input will be larger. Similarly, the wavelength of finite depth waves is less than in deep water and hence the wave slope is larger. Thus the dissipation could also be expected to be larger than in deep water. The altered magnitude of these source terms, together with bottom interactions such as friction all have the potential to alter the source term balance and hence the form of the directional spreading. Under deep water conditions it appears that the nonlinear term,  $S_{nl}$  plays the dominant role in determining the directional spreading (Hasselmann et al., 1980; Donelan et al., 1985; Banner and Young, 1994). It is reasonable to assume that  $S_{nl}$  plays, at least a significant role, if not a dominant one in finite depth conditions.

In order to determine whether  $S_{nl}$  is a possible cause for the broader spreading noted in the present finite depth data compared to the Donelan et al. (1985) deep water data, the directional coupling inherent in this term was examined. The nonlinear source term is most readily expressed in terms of the wavenumber spectrum  $F(\underline{k})$ , where  $\underline{k}$  is the

wavenumber vector. This form can be related to the previously used directional frequency spectrum through the identity:  $\int F(\underline{k})d\underline{k} = \int F(f,\theta)dfd\theta$ . The action density can be expressed in terms of the wavenumber spectrum as  $n(\underline{k}) = F(\underline{k})/\omega$ , where  $\omega = 2\pi f$ . Hasselmann (1963) determined the evolution of  $n$  due to the resonate interaction of four wavenumber components as

$$\frac{\partial n_1}{\partial t} = \iiint G(\underline{k}_1, \underline{k}_2, \underline{k}_3, \underline{k}_4) \times \delta(\underline{k}_1 + \underline{k}_2 - \underline{k}_3 - \underline{k}_4) \times \delta(\omega_1 + \omega_2 - \omega_3 - \omega_4) \times [n_1 n_3 (n_4 - n_2) + n_2 n_4 (n_3 - n_1)] d\underline{k}_1 d\underline{k}_2 d\underline{k}_3 \tag{17}$$

Eq. (17) represents the rate of change of action density  $n_1 = n(\underline{k}_1)$  as a result of resonant nonlinear interactions with spectral components at wavenumbers  $\underline{k}_2, \underline{k}_3$  and  $\underline{k}_4$ . The delta functions in Eq. (17) ensure that only components which satisfy the resonance conditions  $\underline{k}_1 + \underline{k}_2 = \underline{k}_3 + \underline{k}_4$  and  $\omega_1 + \omega_2 = \omega_3 + \omega_4$  contribute to the energy exchange. The coupling coefficient  $G$  (Herterich and Hasselmann, 1980) describes the strength of the interaction. Rather than evaluate the full integral, which is computationally expensive, interest here centres on evaluation of the various terms comprising Eq. (17), to determine whether nonlinear interactions could be responsible for broader spreading in water of finite depth.

In particular, attention is focused on which spectral components satisfy the resonance interactions defined by the delta functions in Eq. (17) and the strength of the interactions for these components as specified by the coupling coefficient,  $G$ . The number of

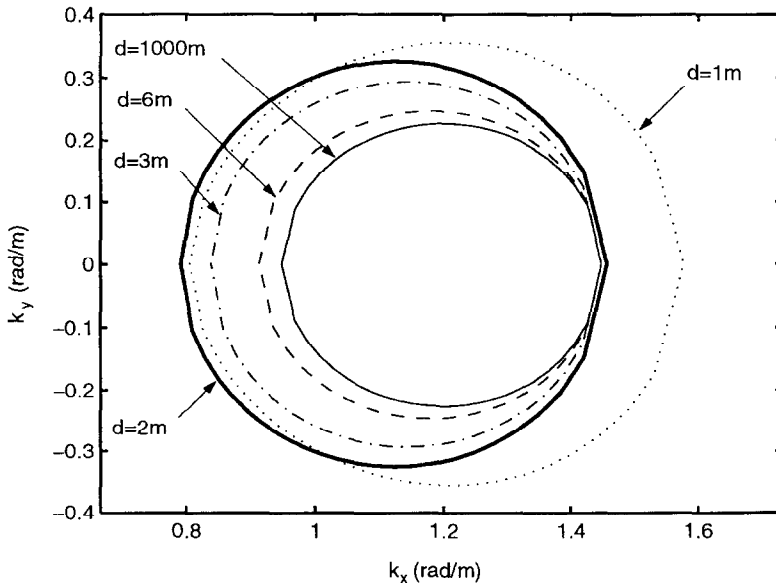


Fig. 11. Loci of the values of  $\underline{k}_2$  which satisfy the resonance conditions in Eq. (17) for  $f_1 = 0.3$  Hz and  $f_3 = 0.6$  Hz. Both  $f_1$  and  $f_3$  are directed parallel to the  $x$  axis. Loci are shown for a number of water depths, as marked.

wavenumber components which can satisfy the resonance conditions is enormous, and the visualization of these components in multi-dimensional wavenumber space is a significant problem. Webb (1978) has shown that for a particular selection of  $\underline{k}_1$  and  $\underline{k}_3$ , the loci of the terminating points of the vectors  $\underline{k}_2$  and  $\underline{k}_4$  which satisfy the resonance conditions will trace out two “egg”-shaped loci in wavenumber space. Examples of this presentation are given by Resio and Perrie (1991) and Young and Van Vledder (1993).

Due to the depth dependence of the dispersion relationship, the actual components which satisfy the resonance conditions will vary with water depth. Fig. 11 shows the loci of the values of  $\underline{k}_2$  as a function of water depth for the case where  $f_1 = 0.3$  Hz ( $\omega_1 = 2\pi f_1$ ) and  $f_3 = 0.6$  Hz. Both  $f_1$  and  $f_3$  are directed along the  $x$  axis of the diagram. These values of  $f_1$  and  $f_2$  were chosen since  $f_p \approx 0.3$  Hz is typical of the present data set. For this combination of  $f_1$  and  $f_3$ , only values of  $\underline{k}_2$  which lie on the locus for that depth will satisfy the resonance conditions and interact nonlinearly to transfer energy. The loci of  $\underline{k}_4$  are not shown here but will be identical in shape to those of  $\underline{k}_2$ , although displaced along the  $x$  axis.

Since the measured data have been presented in frequency space it was deemed appropriate to hold  $f_1$  and  $f_3$  constant as the depth varied in Fig. 11 rather than keep  $|\underline{k}_1|$  and  $|\underline{k}_3|$  constant. The resulting loci gradually increase in size as the depth decreases. Therefore, wavenumbers more widely separated in both magnitude and direction have the potential to interact in shallow water compared to deep. Although only one combination of  $\underline{k}_1$ ,  $\underline{k}_3$  is presented here, the same general trend holds for other combinations. As the water depth decreases, wavenumber components separated by progressively larger angles can satisfy the resonance conditions and potentially interact nonlinearly.

The potential implications of these results for directional spreading are shown in Fig.

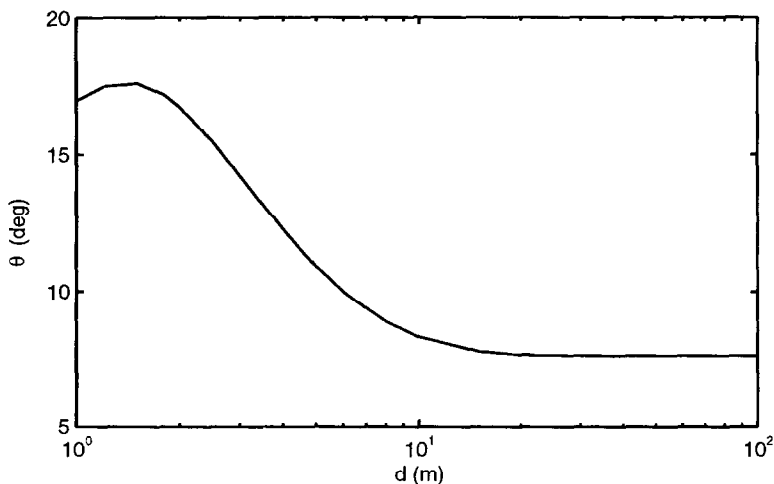


Fig. 12. The angle  $\theta$  made between the  $x$  axis and the component  $f_2 = 0.5$  Hz for the values of  $f_1$  and  $f_3$  used in Fig. 11 as a function of water depth,  $d$ .

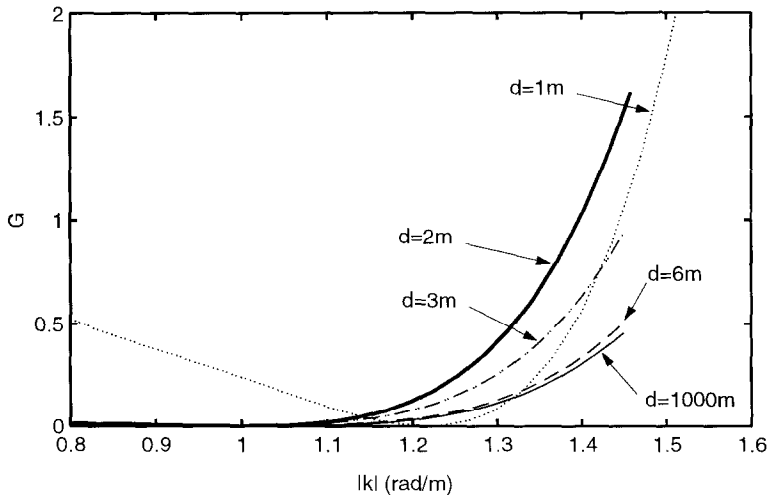


Fig. 13. Values of the coupling coefficient,  $G$  (Eq. (17)) as a function of  $|k_2|$  as shown on Fig. 11. Values are shown for the same water depths depicted in Fig. 11.

12. This figure shows the angle relative to the  $x$  axis made by the component with  $f_2 = 0.5$  Hz in Fig. 11 as a function of depth. As the water depth decreases below approximately 10 m, the angle increases, indicating spectral components at progressively larger angles could interact with components in the mean wind direction. At very small depths the directional spread of the coupling again begins to decrease.

In addition to determining the components which satisfy the resonance conditions and thus potentially interact to exchange energy, the strength of the interaction is also important. This can be measured by the coupling coefficient  $G$  in Eq. (17). Fig. 13 shows the magnitude of the coupling coefficient,  $G$  as a function of  $|k_2|$  for each of the loci in Fig. 11. The magnitude of the coupling generally increases with increasing  $|k_2|$ . In addition, however,  $G$  also increases as the water depth decreases. The strength of the nonlinear coupling is larger in shallow water than in deep water.

The more extensive coupling indicated by Figs. 11 and 12, together with the increased strength of the coupling (Fig. 13) could be expected to yield spectra which are more isotropic with energy spread more evenly in both frequency and direction. Such a result is consistent with the broader directional spreading noted in the present finite depth data compared to the Donelan et al. (1985) deep water results. Similarly, the results of Part II showed that the one dimensional spectra of finite depth waves have a more gradual decay with frequency than deep water spectra (i.e.  $f^{-3}$  compared to  $f^{-5}$ ).

## 7. Conclusions

The data set presented in this paper represents the first comprehensive study of the directional spectra of fetch limited finite depth waves. The data were collected with a

high resolution directional array and processed with an MLM analysis. These results were then corrected for the artificial broadening which occurs with all insitu directional measurement systems. Hence, the resulting spectra have high directional resolution.

The results are qualitatively consistent with previous deep water studies. Spectra are narrowest at the spectral peak frequency and broaden at frequencies both greater than and less than the peak. A parametric representation of the general form,  $\cos^2\theta/2$  was found to adequately approximate the data. The exponent  $s$  was found to be a function of  $f/f_p$  (Eq. (15)) with no obvious dependence on inverse wave age,  $U_{10}/C_p$ . The spreading was found to be significantly broader than the deep water results of Donelan et al. (1985). No systematic dependence on the non-dimensional depth parameter  $k_p d$  could be found within the data, although only a very limited range of values of  $k_p d$  was spanned by the data set.

As nonlinear interactions are believed to play an important role in determining the directional spreading of deep water spectra, the potential importance of this term was investigated for finite depth situations. An analysis of the nonlinear interaction integral showed that the coupling of finite depth waves was more broadly spread across the spectrum in both frequency and direction space than in deep water. In addition, the strength of the nonlinear coupling increases with decreasing water depth. Hence, it is possible that nonlinear interactions would lead to finite depth spectra which are more isotropic than their deep water counterparts. The spectra would have broader directional spreading and a more gradual decay of energy with frequency. These conclusions are consistent with the directional spectra presented in this study as well as the one-dimensional spectra reported in Part II.

## Acknowledgements

Numerous members of the technical staff of the Dept. of Civil Engineering, Univ. College, UNSW have made enormous contributions to the success of this large field experiment. Mary Dalton and Peter McMahon of our electronics section have designed and constructed all electronics used in the project, the reliability of the instrumentation speaks volumes for their skills. The support towers, central platform and numerous other components were constructed by John MacLeod, Doug Collier and Bernie Miller. In addition, numerous other members of staff have assisted in the deployment and maintenance of instruments. They include: Graham Johnston, Jon Delaney, Terry Lutze, David Sharp and Jim Baxter. The project could not have been successful without the significant contributions from this large and very skilled group of people. The project was funded by the Australian Research Council, without which it would have been impossible. This contribution is gratefully acknowledged.

## References

- Banner, M.L., 1990. Equilibrium spectra of wind waves. *J. Phys. Oceanogr.*, 20: 966–984.
- Banner, M.L. and Young, I.R., 1994. Modelling spectral dissipation in the evolution of wind waves — Part 1. Assessment of existing model performance. *J. Phys. Oceanogr.*, 24: 1550–1671.

- Buchan, S.J., Steedman, R.K., Stroud, S.A. and Provis, D.G., 1984. A shallow water directional wave recorder. In: 20th Int. Conf. on Coastal Engineering, Houston, TX, pp. 287–303.
- Cote, L.J., Davis, J.O., Marks, W., McGough, R.J., Mehr, E., Pierson, W.J., Ropek, J.F., Stephenson, G. and Vetter, R.C., 1960. The directional spectrum of wind-generated sea as determined from data obtained by the stereo wave observation project. Meteor. Pap. New York Univ., College of Engineering, 2, 6, 88 pp.
- Donelan, M.A., Hamilton, J. and Hui, W.H., 1985. Directional spectra of wind-generated waves. Philos. Trans. R. Soc. London, A315: 509–562.
- Ewing, J.A. and Laing, A.K., 1987. Directional spectra of seas near full development. J. Phys. Oceanogr., 17: 1696–1706.
- Fontanel, A. and De Staerke, D., 1980. Spectres directionnels de vagues en mer du Nord. Images du radar de SEASAT. In: Climatologie de la Mer, Conference Internationale, Paris, pp. 363–383.
- Forristall, G.Z., Ward, E.G., Cardone, V.J. and Borgmann, L.E., 1978. The directional spectra and kinematics of surface gravity waves in tropical storm Delia. J. Phys. Oceanogr., 8: 888–909.
- Garrett, J., 1970. Field observations of frequency domain statistics and nonlinear effects in wind-generated ocean waves. Thesis, University of British Columbia, 176 pp.
- Gelci, R., Cazalé, H. and Vassal, J., 1957. Préviation de la houle. La méthode des densités spectroangulaires. Bull. Inform. Comité Central Oceanogr. d'Etude Côtes, 9, pp. 416–435.
- Herterich, K. and Hasselmann, K., 1980. A similarity relation for the nonlinear energy transfer in a gravity-wave spectrum. J. Fluid Mech., 97: 215–224.
- Hasselmann, K., 1960. Grundgleichungen der Seegangsvoraussage. Schiffstechnik, 7(39): 191–195.
- Hasselmann, K., 1963. On the non-linear energy transfer in a gravity-wave spectrum, Part 2. Conservation theorems; wave-particle analogy; irreversibility. J. Fluid Mech., 15: 273–281.
- Hasselmann, D.E., Dunkel, M. and Ewing, J.A., 1980. Directional wave spectra observed during JONSWAP 1973. J. Phys. Oceanogr., 10(8): 1264–1280.
- Holthuijsen, L.H., 1983. Observations of the directional distribution of ocean-wave energy in fetch-limited conditions. J. Phys. Oceanogr., 13(2): 191–207.
- Irani, G.B., Gotwols, B.L. and Bjerkaas, A.W., 1981. Ocean wave dynamics test: results and interpretations. Rep. No. STD-R-537, The Johns Hopkins University, Applied Physics Laboratory, 202 pp.
- Isobe, M., Kondo, K. and Horikawa, K., 1984. Extension of MLM for estimating directional wave spectrum. In: Symp. on Description and Modelling of Directional Seas, DHI and MMI, Copenhagen, pp. 1–15.
- Kobune, K., Sasaki, H., and Hashimo, N., 1985. Characteristics of ocean waves off Cape Nojima in the northwest Pacific, measured with a discus buoy. Rep. Port Harbour Res. Inst. Jpn., 24: 3–30.
- Longuet-Higgins, M.S., Cartwright, D.E. and Smith, N.D., 1963. Observations of the directional spectrum of sea waves using the motions of a floating buoy. In: Ocean Wave Spectra. Prentice Hall, Englewood Cliffs, NJ, pp. 111–136.
- McLeish, W., Ross, D., Shuchman, R.A., Teleki, P.G., Hsiao, S.V., Shemdin, O.H. and Brown, W.E., 1980. Synthetic aperture radar imaging of ocean waves: comparison with wave measurements. J. Geophys. Res., 85: 5003–5011.
- Mitsuyasu, H., Tsai, F., Suhara, T., Mizuno, S., Onkusu, M., Honda, T. and Rukiiski, K., 1975. Observations of the directional spectrum of ocean waves using a cloverleaf buoy. J. Phys. Oceanogr., 5: 751–761.
- Pawka, S.S., Hsiao, S.V., Shemdin, O.H. and Inman, D.L., 1980. Comparisons between wave directional spectra from SAR and pressure sensor arrays. J. Geophys. Res., 85: 4987–4995.
- Press, W.H., Flannery, B.P., Teukolsky, S.A. and Vetterling, W.T., 1986. Numerical Recipes. Cambridge University Press, 818 pp.
- Resio, D. and Perrie, W., 1991. A numerical study of nonlinear energy fluxes due to wave-wave interactions. Part I: Methodology and basic results. J. Fluid Mech., 223: 609–629.
- Schuler, D.L., 1978. Remote sensing of directional gravity wave spectra and surface currents using microwave dual-frequency radar. Radio Sci., 13: 321–331.
- Trizna, D.B., Bogle, R.W., Moore, J.C. and Howe, C.M., 1980. Observation by H.F. Radar of the Phillips resonance mechanism for generation of wind waves. J. Geophys. Res., 85: 4946–4956.
- Tyler, G.L., Teague, C.C., Stewart, R.H., Peterson, A.M., Munk, W.H. and Joy, J.W., 1974. Wave directional spectra from synthetic aperture observations of radio scatter. Deep Sea Res., 21: 989–1016.
- Webb, D.J., 1978. Non-linear transfers between sea waves. Deep Sea Res., 25: 279–298.

- Willebrand, J., 1975. Energy transport in a nonlinear and inhomogeneous random wave field. *J. Fluid Mech.*, 70: 113–126.
- Wu, J., 1977. Directional slope and curvature distributions of wind waves. *J. Fluid Mech.*, 79: 463–480.
- Young, I.R., 1994. On the measurement of directional wave spectra. *Appl. Ocean Res.*, 16: 283–294.
- Young, I.R., Rosenthal, W. and Ziemer, F., 1985. Marine radar measurements of waves and currents during turning winds. *Dtsch. Hydrogr. Z.*, 38: 23–38.
- Young, I.R. and Van Vledder, G.P., 1993. A review of the central role of nonlinear interactions in wind-wave evolution. *Philos. Trans. R. Soc. Lond.*, A342: 505–524.
- Young, I.R. and Verhagen, L.A., 1996a. The growth of fetch limited waves in water of finite depth. Part 1. Total energy and peak frequency. *Coastal Eng.*, 29 (1996) 47–78 (this issue).
- Young, I.R. and Verhagen, L.A., 1996b. The growth of fetch limited waves in water of finite depth. Part 2. Spectral evolution. *Coastal Eng.*, 29 (1996) 70–99 (this issue).